Magnetohydrodynamic modeling of the global solar corona*

Zoran Mikić,† Jon A. Linker, Dalton D. Schnack, Roberto Lionello, and Alfonso Tarditi
Science Applications International Corporation, 10260 Campus Point Drive, San Diego, California 92121

(Received 19 November 1998; accepted 21 January 1999)

A three-dimensional magnetohydrodynamic model of the global solar corona is described. The model uses observed photospheric magnetic fields as a boundary condition. A version of the model with a polytropic energy equation is used to interpret solar observations, including eclipse images of the corona, Ulysses spacecraft measurements of the interplanetary magnetic field, and coronal hole boundaries from Kitt Peak He 10 830 Å maps and extreme ultraviolet images from the Solar Heliospheric Observatory. Observed magnetic fields are used as a boundary condition to model the evolution of the solar corona during the period February 1997–March 1998. A model with an improved energy equation and Alfvén waves that is better able to model the solar wind is also presented. © *1999 American Institute of Physics.* [S1070-664X(99)94805-X]

I. INTRODUCTION

The sophistication of models of the solar corona has increased considerably since the idealized models of the 1980's (e.g., see Mikić[1] and Low[2] for examples of early models). This has been brought about by a confluence of three key elements. First, the collection of high-resolution observations of the Sun, both in space and time, has grown tremendously. For example, consider the changes in our perception of the Sun brought about by Yohkoh[3] images of the x-ray Sun; Ulysses measurements of the polar solar wind;[4] high-resolution white-light movies of solar granulation; high-resolution vector magnetographs of active regions;[5] Solar Heliospheric Observatory (SOHO) high-resolution images of the photospheric magnetic field, white-light coronagraph, and extreme ultraviolet (EUV) images of the corona, and energetic particle and solar wind composition measurements. The space-based observations are nicely complemented by an extensive archive of ground-based observations [in particular, magnetic field measurements at Kitt Peak National Solar Observatory (NSOKP) and Wilcox Solar Observatory (WSO); He 10 830 Å observations of coronal hole boundaries at NSOKP; Mauna Loa coronagraph images; and interplanetary scintillation (IPS) measurements]. Second, the power and availability of supercomputers has made two- and three-dimensional modeling routine; the increase in computing power that massive parallelism promises will extend the possibilities for realistic modeling even further. Third, the sophistication of the models themselves, both in their geometrical realism and the physics that has been included, has matured significantly.

The application of magnetohydrodynamic (MHD) coronal models to these solar observations has begun to exploit this confluence of capabilities. It is now possible to make direct comparisons between observations and models of the solar corona, as illustrated below. The development of this modeling capability is especially timely, since the observations from present missions [including the recently launched transition-region and coronal explorer (TRACE) mission] and coming missions [Solar-B, set for launch in 2004, will provide high-resolution measurements of vector magnetic fields, x-ray, and EUV emission in active regions; the Solar-Terrestrial Relations Observatory (STEREO) will take coronal images from multiple viewpoints; and Solar Probe will explore the inner solar corona] have challenged our understanding of the Sun.

To fully exploit the available data it is necessary to apply sophisticated models that use observational data as inputs and that produce observable quantities as outputs. Through this interplay of observations and theory we can improve our understanding of the Sun and heliosphere. In this paper we show examples of how large-scale models of the solar corona can be used to make detailed comparisons with observations.

II. POLYTROPIC MHD MODEL

A self-consistent description of the large-scale solar corona requires the coupled interaction of magnetic, plasma, and solar gravity forces, including the effect of the solar wind. For simplicity we first describe a ''polytropic model,'' in which an adiabatic energy equation with a reduced polytropic index γ (i.e., smaller than 5/3) is used.[6] This is a crude way of modeling the complicated thermodynamics in the corona with a simple energy equation. The primary motivation for using a reduced γ is the fact that the temperature in the corona does not vary substantially (the limit $\gamma \rightarrow 1$ corresponds to an isothermal plasma). A typical choice, used here, is $\gamma = 1.05$. Detailed comparisons of our results with coronal observations indicate that while this model matches many features of the corona (as shown below), it is not accurate enough to quantitatively reproduce the properties of the corona and solar wind. In particular, this simple model fails to reproduce the fast (~800 km/s) and slow (~400 km/s) solar wind streams[4] that are measured at Earth, nor does it reproduce the contrast in density and temperature that is observed

*Paper D2I2.4 Bull. Am. Phys. Soc. **43**, 1700 (1998).
†Invited speaker.

between streamers and coronal holes. An improved model that does not suffer from these limitations is presented in Sec. IV.

Theoretical arguments indicate that magnetic reconnection is crucial to describe the structure and dynamics of the solar corona.[7–9] Yohkoh observations also present strong evidence for the importance of magnetic reconnection.[10] We therefore include the effect of plasma resistivity (with the important caveat that numerical models require the resistivity to be enhanced compared to coronal values[11]). In the resistive MHD model, the coronal plasma is described by the following equations:

$$\nabla\times\mathbf{B}=\frac{4\pi}{c}\mathbf{J}, \tag{1}$$

$$\nabla\times\mathbf{E}=-\frac{1}{c}\frac{\partial\mathbf{B}}{\partial t}, \tag{2}$$

$$\mathbf{E}+\frac{1}{c}\mathbf{v}\times\mathbf{B}=\eta\mathbf{J}, \tag{3}$$

$$\frac{\partial\rho}{\partial t}+\nabla\cdot(\rho\mathbf{v})=0, \tag{4}$$

$$\rho\left(\frac{\partial\mathbf{v}}{\partial t}+\mathbf{v}\cdot\nabla\mathbf{v}\right)=\frac{1}{c}\mathbf{J}\times\mathbf{B}-\nabla p-\nabla p_w+\rho\mathbf{g}+\nabla\cdot(\nu\rho\nabla\mathbf{v}), \tag{5}$$

$$\frac{\partial p}{\partial t}+\nabla\cdot(p\mathbf{v})=(\gamma-1)(-p\nabla\cdot\mathbf{v}+S), \tag{6}$$

where $\mathbf{B}$ is the magnetic field, $\mathbf{J}$ is the electric current density, $\mathbf{E}$ is the electric field, ρ, $\mathbf{v}$, p, and T are the plasma mass density, velocity, pressure, and temperature, and the wave pressure p_w represents the acceleration due to Alfvén waves (see Sec. IV). The gravitational acceleration is $\mathbf{g}=-g_0\hat{\mathbf{r}}/r^2$, η is the resistivity, ν is the kinematic viscosity, and S represents energy source terms. The plasma pressure is $p=(n_e+n_p)kT$, where n_e and n_p are the electron and proton densities; for a hydrogen plasma, $n_e=n_p$. The polytropic model is defined by setting $\gamma=1.05$ and $S=0$ in Eq. (6), and zero Alfvén wave pressure in Eq. (5), $p_w=0$.

We have developed a three-dimensional code (3D)[11,12] to solve the MHD equations (1)–(6) in spherical coordinates (r,θ,ϕ). This code has been used extensively to model the 2D and 3D corona, including the structure of helmet streamers,[13–15] coronal mass ejections,[11,16–19] and the long-term evolution of the solar corona and heliospheric current sheet (see Sec. III). Related methods have been developed by Usmanov[20,21] and Pisanko.[22] The following boundary conditions are used.[14,17,19] The radial magnetic field B_r is specified at the solar surface $r=R_s$ (e.g., from synoptic magnetic field observations at NSOKP and WSO, or from full-disk magnetograms). This field may evolve in time (see Sec. III). The boundary conditions on the velocity are determined from the characteristic equations along $\mathbf{B}$. The plasma pressure, as well as the plasma density in regions where the radial velocity is positive, are specified at $r=R_s$. (In the calculations presented here, the boundary values of p and ρ were chosen to be uniform.) Characteristic equations are also used at the upper radial boundary, which is placed beyond the sonic and Alfvén points (typically at $r=30R_s$, although we have performed simulations that have included Earth's orbit in the domain,[19] and beyond).

Typical parameters for the quiet corona[23] yield a value for the Lundquist number of $S\sim10^{13}$. Since it is not possible to perform well-resolved numerical computations[11] at this large value of S, we must content ourselves with calculations at lower, but still substantial, values of $S\sim10^3-10^4$. We also use finite viscosity ν corresponding to a viscous diffusion time $\tau_\nu\sim10^2-10^3\tau_A$, where $\tau_\nu=R_s^2/\nu$, $\tau_A=R_s/v_A$ is the Alfvén transit time, and v_A is the Alfvén speed. At the lower values of S used in the simulations we expect that the static current sheets in the solution (e.g., the heliospheric current sheet) will form in approximately the correct location, but will be broader than those in the corona.

Pneuman and Kopp[24] developed the first 2D model of helmet streamer equilibria by solving the steady-state MHD equations. Our approach, and that used in many other calculations, is to integrate the time-dependent MHD equations to steady state.[25–29] The following initial condition is used. For the given B_r distribution at $r=R_s$, a potential magnetic field $(\nabla\times\mathbf{B}=0)$ is calculated in the corona, and a transonic spherically symmetric wind solution[6] is used to specify p, ρ, and $\mathbf{v}$. The MHD equations are integrated in time until the plasma and magnetic fields settle into equilibrium. The final state has closed magnetic field regions (helmet streamers), where the solar wind plasma is trapped, surrounded by open fields (coronal holes), where the solar wind flows freely along magnetic field lines, accelerating to supersonic speeds. This model has also been used to study dynamic events in the corona, including coronal mass ejections (CMEs);[11,16–19] this aspect will not be addressed in the present paper.

A. Comparison with eclipse images

Total solar eclipses offer an excellent opportunity to observe coronal streamers. The white-light polarized brightness of the corona that can be measured during an eclipse can be simulated from our MHD solution by integrating the electron density along the line of sight in the plane of the sky (convolved with a scattering function[30] and filtered with a radially graded filter to mimic the effect of instrument ''vignetting''). Our first attempt to model the corona[13,14] was performed subsequent to the eclipse of 3 November 1994, observed in Chile. Since then, we have made three *predictions*, before the actual eclipse date, using magnetic field data from the previous solar rotation, for the eclipses of 25 October 1995,[19] seen in Vietnam and India; 9 March 1997, seen in Siberia, China, and Mongolia; and 26 February 1998, seen in the Caribbean. These predictions were published on the World Wide Web prior to the eclipses. We used NSOKP and WSO synoptic magnetic field maps for the calculations. The comparison of simulated polarization brightness with eclipse images is shown in Fig. 1. Comparisons with Mauna Loa MK3 coronagraph observations on several days during the solar rotations surrounding the eclipses have confirmed that the basic large-scale three-dimensional structure of the streamer belt has been captured in the model. The agreement between the model and the eclipse images is quite good,

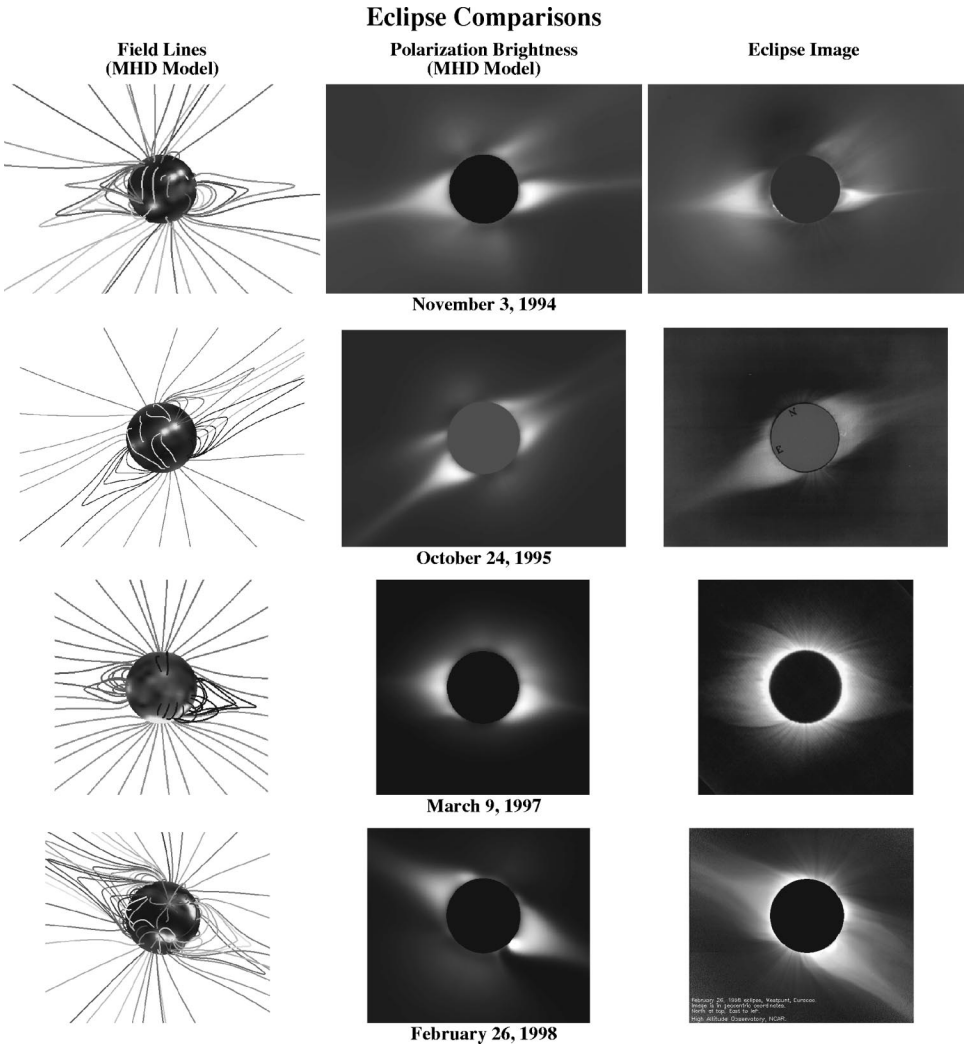

FIG. 1. Comparison of MHD computations of the solar corona with total solar eclipse observations. The 3 November 1994 eclipse was modeled subsequent to the eclipse; the other three calculations were predictions, performed in advance of the eclipse date, using magnetic field data from NSOKP and WSO. All the images are shown with geocentric north up, except for the 1997 eclipse, which has solar north up. (The sources of the eclipse images are listed in the Acknowledgments section.)

especially considering that three of the cases are predictions. Note, however, that these eclipses occurred close to solar minimum, when the large-scale structure of the Sun changes slowly between solar rotations. We are planning to predict the state of the corona during the forthcoming total solar eclipse in August 1999, which will be seen in central and eastern Europe, the Middle East, and western Asia. This prediction will be our most challenging yet, since this eclipse will occur close to solar maximum, when the structure of the corona is expected to be considerably more complicated, and changing more rapidly, than for the cases we have simulated previously.

B. Comparison with Ulysses measurements

The coronal magnetic field not only defines the structure of the solar corona, but the position of the heliospheric current sheet (HCS), and the regions of fast and slow solar wind as well. Understanding how the Sun influences the structure of the inner heliosphere requires an accurate mapping of the photospheric magnetic field into the corona and beyond. Source–surface models[31–38] provide predictions of the structure of the magnetic field in the corona and heliosphere. Source–surface models are relatively simple to apply, and have yielded important insights into the structure of the heliosphere, but a number of aspects of the Ulysses data are not described well by these models.[39–41] In particular, the latitudinal profile of the radial magnetic field and the extent of the HCS predicted by source–surface models show significant discrepancies from Ulysses observations. During May–June 1993 the Ulysses spacecraft, which was located at 30 °S latitude, ceased to observe sector boundary (i.e., HCS) crossings.[39] The ''classic'' Wilcox source–surface model[34,35] predicted that Ulysses would cross the heliospheric current sheet, whereas the MHD simulation correctly predicted no crossing.[13,19] The radial magnetic field from the MHD computation shows little latitudinal variation, consistent with Ulysses observations, in contrast to the source–surface model result. This agreement with Ulysses data indi-

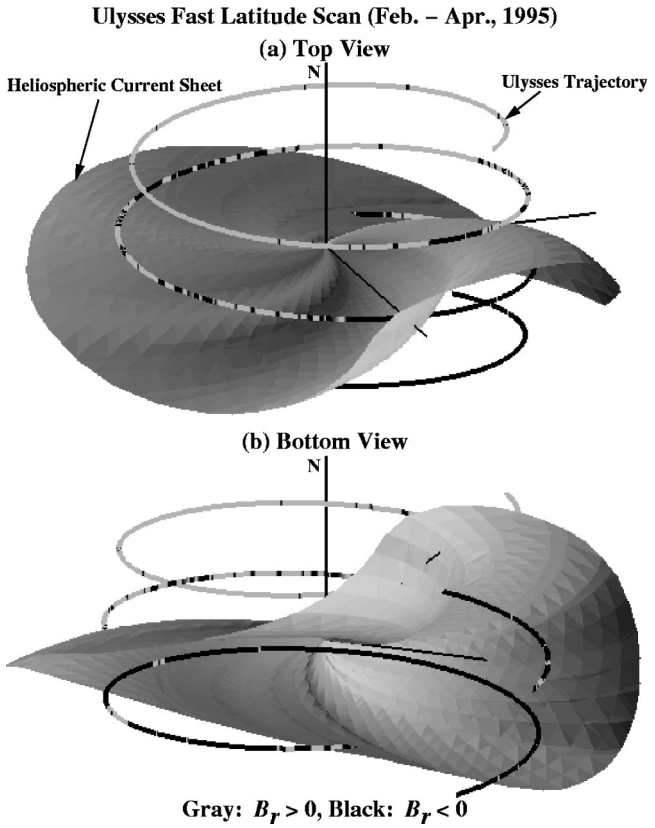

FIG. 2. Heliospheric current sheet for Carrington rotation 1892 and the Ulysses trajectory (February–April, 1995), in the rotating frame of the Sun. The color of the trajectory indicates the polarity of the magnetic field, as measured by Ulysses. Two views of the HCS are shown, (a) from above the HCS, and (b) from below the HCS. The large-scale polarity of the magnetic field is consistent with that predicted by the MHD model (positive above the HCS, negative below); the short-scale differences may be due to Alfvén waves and to structures that have not been included in the limited-resolution calculation. The MHD calculation was performed up to 400 solar radii. Ulysses was at a distance of ~1.4 astronomical units (AU) from the Sun at this time.

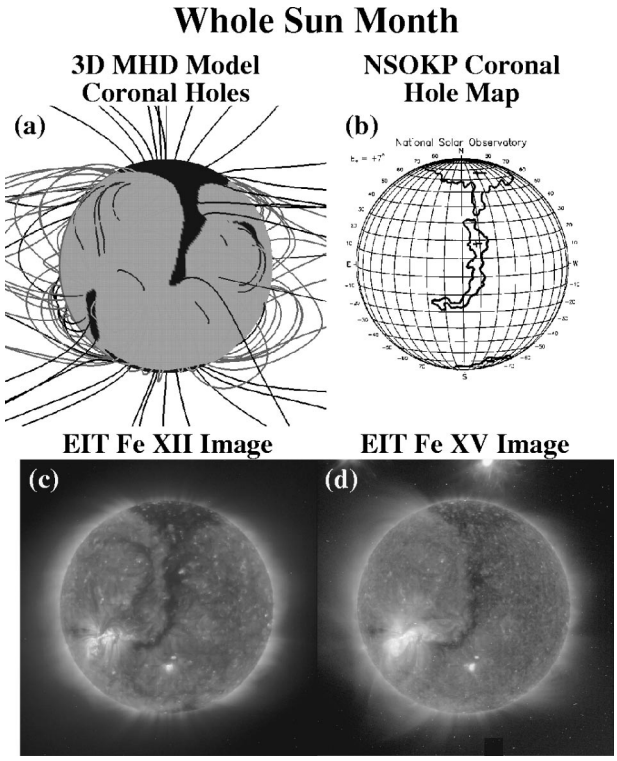

FIG. 3. Comparison of the MHD model with coronal holes seen in disk measurements on 27 August 1996. The ''elephant's trunk'' coronal hole (extending from the north pole past the equator) can be seen in both the simulation and the data. The NSOKP coronal hole map is deduced from He 10 830 Å images. The SOHO/EIT images are in EUV wavelengths.

cates that MHD computations may provide a better way of mapping phenomena in the solar wind back to their origin in the solar corona.

The Ulysses fast latitude scan (February–April, 1995) was a time period during which the Ulysses spacecraft traversed rapidly from southern polar latitudes of the Sun to northern polar latitudes, and offers another opportunity to test the MHD model.[19] Figure 2 shows that the HCS structure predicted by the MHD model generally matches Ulysses measurements of the magnetic field polarity. A more detailed analysis of the HCS crossings[19] shows consistency between the measurements and the model. We also used the MHD model (by tracing magnetic field lines back to the Sun, in conjunction with ballistic mapping in the region outside the computation) to deduce the solar origin of plasma observed at Ulysses. The results suggest that the fast solar wind generally comes from deeper within coronal holes than does the slow wind.[42]

C. Whole Sun Month comparison

MHD modeling is particularly useful for studying the solar corona and solar wind when a coordinated set of observations is available, since it can help to synthesize different measurements into a coherent picture. The Whole Sun Month campaign (WSM; 10 August–8 September, 1996) brought together a wide range of space and ground-based observations during solar minimum. Our MHD model was used to interpret coronagraph and EUV images,[15,43] interplanetary scintillation measurements of the solar wind speed,[44] and the structure of corotating interaction regions (CIRs) as deduced from energetic particle measurements.[45]

The ''elephant's trunk'' coronal hole, an equatorial extension of the northern polar coronal hole, named on account of its shape, was perhaps the most conspicuous coronal feature observed during WSM, and was apparent in several different wavelengths, including SOHO Extreme Ultraviolet Imaging Telescope (EIT) images, NSOKP He 10 830 Å maps, and Yohkoh soft x rays. It was most visible around 26–27 August 1996. Figure 3 shows tracings of the magnetic field from the MHD model as they would appear on 27 August 1996, with coronal holes (i.e., regions with open field lines, colored black) and closed-field regions (gray) mapped on the surface of the Sun. For comparison, NSOKP coronal hole boundaries and SOHO/EIT EUV images are also shown. It is apparent that the MHD model reproduces the elephant's trunk coronal hole,[15] although the observations show that the coronal hole extends to lower latitudes than predicted by the model.

We also investigated the solar origins of features observed by the Ulysses and Wind[46] spacecraft during WSM. The slow solar wind maps back close to coronal hole bound-

aries, while the fast wind typically comes from deeper within coronal holes, a pattern similar to that seen during the Ulysses fast latitude scan (Sec. II B). The model also predicts HCS crossings by Wind (but not by Ulysses) during the WSM time period.[15] Wind HCS crossings similar to those predicted were in fact observed.

III. MODELING CORONAL EVOLUTION

In the previous section we used our model to find steady-state coronal solutions for a given distribution of photospheric magnetic field. This approach is limited to the study of the long-time properties of the solar corona. In reality, even if we neglect large-scale eruptions like coronal mass ejections, the corona is changing continuously, even during times of solar minimum. This changing structure is driven by changes in the photospheric magnetic field; active regions emerge and disperse continuously during the solar cycle. We have extended our model to incorporate the evolution of the photospheric magnetic field, so that we can now follow the evolution of the corona. This gives us the capability to study the long-term evolution of the corona (as shown below), the detailed evolution during a time period of interest (e.g., during Whole Sun Month), as well as the ability to study theoretically the coronal consequences of changes in photospheric magnetic flux.

When we seek steady-state solutions of Eqs. (1)–(6), we set the tangential component of the electric field at the boundary, $\mathbf{E}_{t_0}$, to zero. This keeps B_{r_0} (B_r at $r=R_s$) fixed in time. To make the flux evolve to match observed changes, it is necessary to specify a nonzero $\mathbf{E}_{t_0}$. In general, $\mathbf{E}_{t_0}$ can be expressed as $\nabla_t\times\Psi\hat{\mathbf{r}}+\nabla_t\Phi$, where Ψ and Φ are arbitrary functions (of θ and ϕ) and ∇_t indicates tangential derivatives (in the θ-ϕ plane at $r=R_s$). The potential Φ changes $\mathbf{E}_{t_0}$ without changing the flux B_{r0}, and can be used to control the transverse magnetic field (i.e., the shear and the normal electric current), whereas the potential Ψ changes the flux. Since line-of-sight magnetograms do not provide information about the transverse component of the magnetic field, we only consider the case $\Phi=0$ here. Note that a nonzero Φ can be used to introduce shear into the field[18] and to match vector magnetic field measurements.[47] The potential Ψ is obtained by solving the equation $c\nabla_t^2\Psi=\partial B_{r_0}/\partial t$. Therefore, Ψ is evaluated as new solar magnetic field measurements become available, specifying the evolution of $\mathbf{E}_{t_0}$, which is used as a boundary condition for the MHD equations.

Thus, rather than computing a sequence of steady-state solutions for each set of magnetic field boundary values, our time-dependent MHD model now represents the actual state of the corona corresponding to the evolving magnetic field measured on the surface of the Sun. We have used a sequence of synoptic Kitt Peak magnetic field observations to study the evolution of the corona during the period 1 February 1997–18 March 1998 (14 Carrington rotations). This time interval covers the beginning of the new solar cycle, as the Sun emerges from solar minimum, and includes the emergence of high-latitude active regions. To model the evolution over a time interval of over a year is computationally prohibitive at present. In order to study the quasistatic evolution of the corona, we changed the photospheric magnetic field at a rate that was enhanced by approximately ten times compared to real time.[48] This approximation makes it impossible to study the detailed evolution of individual events, though it is still meaningful to study the quasistatic evolution of the large-scale structure of the corona. Figure 4 shows the evolution of the streamer structure, the coronal hole boundaries, and the heliospheric current sheet during this time period. Note the increase in complexity of the coronal magnetic field as the Sun emerges from solar minimum. The output of this model can easily be compared with coronal observations, as was demonstrated in Sec. II.

IV. IMPROVED MHD MODEL

Detailed comparisons of our model with observations, such as those presented in Sec. II, have forced us to confront the limitations of the polytropic MHD model. While the polytropic model matches many features of the corona, it does not reproduce the properties of the fast and slow solar wind or the large contrast in density and temperature between streamers and coronal holes. We have improved the model by including the physical mechanisms that describe the transport of energy in the corona and solar wind. One-dimensional models have been quite successful, despite their obvious geometrical limitations, in describing this interaction.[49,50] We have improved the energy equation in our model to include the effects of parallel thermal conduction, radiation loss, and parameterized coronal heating, and we have included a self-consistent model for Alfvén wave acceleration. The source term in the energy equation (6) is given by

$$S=-\nabla\cdot\mathbf{q}-n_e n_p Q(T)+H_{\rm ch}+H_d+D, \tag{7}$$

where $H_{\rm ch}$ is the coronal heating source, D is the Alfvén wave dissipation term, $H_d=\eta J^2+\nu\nabla\mathbf{v}:\nabla\mathbf{v}$ represents heating due to viscous and resistive dissipation, and $Q(T)$ is the radiation loss function.[51] In the collisional regime (below $\sim 10R_s$), the heat flux is $\mathbf{q}=-\kappa_\parallel\hat{\mathbf{b}}\hat{\mathbf{b}}\cdot\nabla T$, where $\hat{\mathbf{b}}$ is the unit vector along $\mathbf{B}$, and $\kappa_\parallel=9\times10^7T^{5/2}$ is the Spitzer value of the parallel thermal conductivity. The polytropic index γ now becomes the ratio of specific heats, $\gamma=5/3$. In the collisionless regime (beyond $\sim 10R_s$), the heat flux is modeled by $\mathbf{q}=\alpha n_e kT\mathbf{v}$, where α is a parameter.[52] Since it is presently not known in detail what heats the solar corona,[9] the coronal heating source $H_{\rm ch}$ is a parameterized function. A typical form is

$$H_{\rm ch}=H_0(\theta)\exp[-(r-R_s)/\lambda(\theta)], \tag{8}$$

where $H_0(\theta)$ expresses the latitudinal variation of the volumetric heating, and $\lambda(\theta)$ expresses the latitudinal variation of the scale length. [In practice, the variation can be expressed in terms of the magnetic topology (i.e., a proxy for the open and closed field regions) rather than the latitude θ.]

Since the acceleration of the solar wind by Alfvén waves occurs on spatial and time scales that are below the resolu-

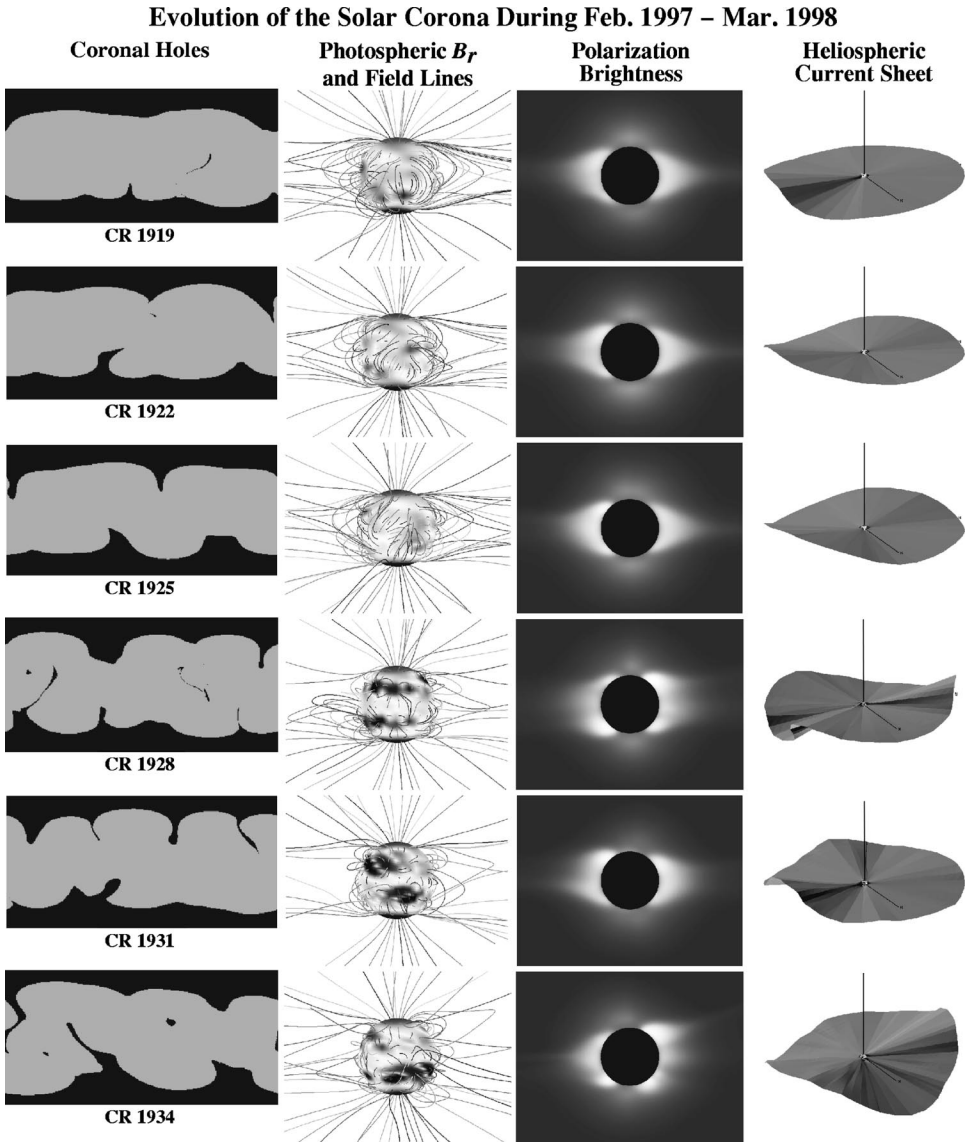

FIG. 4. The changing structure of the solar corona during the period February 1997–March 1998, Carrington rotations (CR) 1919–1934, as illustrated by coronal hole maps (longitude vs latitude, with gray/black indicating closed/open field regions), field line traces with the radial magnetic field shown on the surface of the Sun, polarization brightness, and the shape of the heliospheric current sheet. The HCS is shown up to 30 solar radii. The photospheric magnetic field was set as a time-dependent boundary condition on the 3D MHD simulation using NSOKP synoptic maps.

tion of our global numerical model, the wave pressure p_w is evolved using a WKB approximation[53] for the time-space averaged Alfvén wave energy density ϵ:

$$\frac{\partial \epsilon}{\partial t} + \nabla \cdot \mathbf{F} = \mathbf{v} \cdot \nabla p_w - D, \tag{9}$$

where $\mathbf{F} = (3/2\mathbf{v} + \mathbf{v}_A)\epsilon$ is the Alfvén wave energy flux, $v_A = B/\sqrt{4\pi\rho}$ is the Alfvén speed, and $p_w = \epsilon/2$. The Alfvén wave velocity is $\mathbf{v}_A = \pm \hat{\mathbf{b}} v_A$; in a multidimensional implementation, it is necessary to transport two Alfvén wave fields (waves parallel and antiparallel to **B**), which are combined to give ϵ. The Alfvén wave energy density ϵ is related to the space-time average of the fluctuating component of the magnetic field δB by $\epsilon = \langle \delta B^2 \rangle / 4\pi$. The dissipation term D expresses the nonlinear dissipation of Alfvén waves in interplanetary space and is modeled phenomenologically.[52]

The boundary $r = R_s$ is now chosen to be at the top of the transition region, at a given temperature (say $T_0 = 500\,000$ K). The density at $r = R_s$ is determined by balancing radiation loss, thermal conduction, and heating within the chromosphere and transition region.[49] In this formulation, the only boundary conditions required from observations are on the radial magnetic field. Instead of specifying a nonuniform temperature at the coronal base to express the observed variation of temperature between streamers and coronal holes, as would be required in the polytropic model, we now specify the distribution of coronal heating. By investigating how MHD solutions compare with observations it will be possible to test different coronal heating models, and, eventually, when the coronal heating process is better understood, to relate the heating source to physical quantities.

This formulation has been applied to a 2D (axisymmet-

ric) model of the corona. Extensive tests show that a nonuniform heating profile, together with Alfvén waves, can reproduce the speed, mass flux, density, and temperature of the fast and slow solar wind at Earth. The coronal density contrast is much improved compared to the polytropic model: coronal streamers are 5–10 times denser than coronal holes. The model is presently being extended to 3D.

V. CONCLUSION

The last decade has seen a marked increase in the sophistication of models of the solar corona. Present models have improved geometrical realism, improved physics, are able to use solar observations directly as boundary conditions on the calculations (e.g., measured photospheric magnetic field), and can model the evolving solar corona. We have presented comparisons between a 3D MHD model and observations of coronal and heliospheric structure. The agreement between simulated coronal structure and observations is encouraging, implying that the models are mature enough for detailed analysis. Such 3D models will undoubtedly find increased use in interpreting solar observations and developing up-to-date models of the solar corona. Yet it must be recognized that we have only begun to ''scratch the surface'' of what is possible. Despite these advances, some of the fundamental theoretical questions in solar physics remain unsolved [e.g., what initiates CMEs and flares; what is the relationship between CMEs and flares; how do coronal magnetic structures emerge, evolve, and erupt; what heats the solar corona?]. Continued comparisons of model predictions and observations will help to answer these key questions and provide new insights into the physics of the corona.

ACKNOWLEDGMENTS

The authors thank Dr. Jack Harvey (NSOKP) and Dr. Todd Hoeksema (WSO) for kindly providing us with up-to-date magnetic field data for our eclipse predictions. Kitt Peak synoptic magnetic charts and coronal hole maps are courtesy of NSOKP, which is funded cooperatively by the National Science Foundation (NSF)/National Optical Astronomy Observatories (NOAO), the National Aeronautics and Space Administration (NASA)/Goddard Space Flight Center (GSFC), and the National Oceanic and Atmospheric Administration (NOAA)/Space Environment Center (SEC). EIT data are courtesy of the SOHO EIT consortium. SOHO is a project of international cooperation between NASA and the European Space Agency (ESA). Ulysses magnetic field data were obtained from the National Space Science Data Center. The 1994 and 1998 eclipse images are courtesy of the High Altitude Observatory, National Center for Atmospheric Research (NCAR) Boulder, CO. NCAR is sponsored by NSF. The 1995 eclipse image is courtesy of F. Diego and S. Koutchmy. The 1997 eclipse image is courtesy of Dr. E. Hiei of Meisei University and the National Astronomical Observatory of Japan. This research was supported by NASA Space Physics Theory Program Contract No. NAS5-96081, NASA Supporting Research and Technology Contract Nos. NASW-5017, NASW-4968, and NASW-98030, and NSF Grant Nos. ATM-9320575, ATM-9319517, and AMT-9613834. Computational facilities were provided by the U.S. Department of Energy at the National Energy Research Supercomputer Center and by NSF at the San Diego Supercomputer Center.

[1] Z. Mikić, Phys. Fluids B **2**, 1450 (1990).
[2] B. C. Low, Annu. Rev. Astron. Astrophys. **28**, 491 (1990).
[3] L. Acton, S. Tsuneta, Y. Ogawara, R. Bentley, M. Bruner, R. Canfield, L. Culhane, G. Doschek, E. Hiei, and T. Hirayama, Science **258**, 618 (1992).
[4] D. J. McComas, S. J. Bame, B. L. Barraclough, W. C. Feldman, H. O. Funsten, J. T. Gosling, P. Riley, R. Skoug, A. Balogh, R. Forsyth, B. E. Goldstein, and M. Neugebauer, Geophys. Res. Lett. **25**, 1 (1998).
[5] B. W. Lites, B. C. Low, V. Martínez Pillet, P. Seagraves, A. Skumanich, Z. A. Frank, R. A. Shine, and S. Tsuneta, Astrophys. J. **446**, 877 (1995).
[6] E. N. Parker, *Interplanetary Dynamical Processes* (Wiley, New York, 1963).
[7] E. R. Priest, *Solar Magnetohydrodynamics* (Reidel, Dordrecht, 1982).
[8] E. N. Parker, *Cosmical Magnetic Fields* (Clarendon, Oxford, 1979).
[9] E. N. Parker, *Spontaneous Current Sheets in Magnetic Fields* (Oxford, New York, 1994).
[10] S. Tsuneta, Astrophys. J. **456**, 840 (1996).
[11] Z. Mikić and J. A. Linker, Astrophys. J. **430**, 898 (1994).
[12] The numerical techniques used are similar to those described for a cylindrical code by R. Lionello, Z. Mikić, and D. D. Schnack, J. Comput. Phys. **140**, 172 (1998).
[13] Z. Mikić and J. A. Linker, *Solar Wind Eight: Proceedings of the Eight International Solar Wind Conference*, edited by D. Winterhalter, J. T. Gosling, S. R. Habbal, W. S. Kurth, and M. Neugebauer (American Institute of Physics, Woodbury, NY, 1996), Conf. Proc. Vol. 382, p. 104.
[14] J. A. Linker, Z. Mikić, and D. D. Schnack, *Solar Drivers of Interplanetary and Terrestrial Disturbances*, edited by K. S. Balasubramaniam, S. L. Keil, and R. N. Smartt (Astronomical Society of the Pacific, 1996), Conf. Series Vol. 95, p. 208.
[15] J. A. Linker, Z. Mikić, D. A. Biesecker, R. J. Forsyth, S. E. Gibson, A. J. Lazarus, A. Lecinski, P. Riley, A. Szabo, and B. J. Thompson, ''Magnetohydrodynamic modeling of the solar corona during Whole Sun Month,'' J. Geophys. Res. (in press).
[16] J. A. Linker, Z. Mikić, and D. D. Schnack, *Proceedings of the Third SOHO Workshop—Solar Dynamic Phenomena and Solar Wind Consequences*, Estes Park, CO (European Space Agency, Paris, 1994), SP-373, p. 249.
[17] J. A. Linker and Z. Mikić, Astrophys. J. **438**, L45 (1995).
[18] Z. Mikić and J. A. Linker, *Coronal Mass Ejections*, edited by N. Crooker, J. Joselyn, and J. Feynman (American Geophysical Union, Washington DC, 1997), Geophys. Monograph 99, p. 57.
[19] J. A. Linker and Z. Mikić, *Coronal Mass Ejections*, edited by N. Crooker, J. Joselyn, and J. Feynman (American Geophysical Union, Washington DC, 1997), Geophys. Monograph 99, p. 269.
[20] A. V. Usmanov, *Solar Wind Eight: Proceedings of the Eight International Solar Wind Conference*, edited by D. Winterhalter, J. T. Gosling, S. R. Habbal, W. S. Kurth, and M. Neugebauer (American Institute of Physics, Woodbury, NY, 1996), Conf. Proc. Vol. 382, p. 141.
[21] A. V. Usmanov, B. P. Besser, J. M. Fritzer, and M. L. Goldstein, ''Two-dimensional MHD simulation of the solar corona with WKB Alfvén waves,'' J. Geophys. Res. (submitted).
[22] Y. V. Pisanko, ''A composite MHD model of an expanding corona and its application to the Whole Sun Month campaign,'' J. Geophys. Res. (submitted).
[23] E. N. Parker, Astrophys. J. **264**, 642 (1983).
[24] G. W. Pneuman and R. A. Kopp, Sol. Phys. **18**, 258 (1971).
[25] F. Endler, Ph.D. thesis, Gottingen University, 1971.
[26] R. S. Steinolfson, S. T. Suess, and S. T. Wu, Astrophys. J. **255**, 730 (1982).
[27] H. Washimi, Y. Yoshino, and T. Ogino, Geophys. Res. Lett. **14**, 487 (1987).
[28] J. A. Linker, G. Van Hoven, and D. D. Schnack, Geophys. Res. Lett. **17**, 2281 (1990).
[29] A. H. Wang, S. T. Wu, S. T. Suess, and G. Poletto, Sol. Phys. **147**, 55 (1993).
[30] D. E. Billings, *A Guide to the Solar Corona* (Academic, New York, 1966).
[31] K. H. Schatten, J. M. Wilcox, and N. Ness, Sol. Phys. **6**, 442 (1969).
[32] M. D. Altschuler and G. Newkirk, Sol. Phys. **9**, 131 (1969).
[33] K. H. Schatten, Cosmic Electrodyn. **2**, 232 (1971).

[34]J. T. Hoeksema, J. M. Wilcox, and P. H. Scherrer, J. Geophys. Res. **88**, 9910 (1983).
[35]J. T. Hoeksema, Adv. Space Res. **9**, 141 (1989).
[36]Y.-M. Wang and N. R. Sheeley, Jr., Astrophys. J. **392**, 310 (1992).
[37]Y.-M. Wang and N. R. Sheeley, Jr., Astrophys. J. **447**, L143 (1995).
[38]X. Zhao and J. T. Hoeksema, J. Geophys. Res. **100**, 19 (1995).
[39]E. J. Smith, M. Neugebauer, A. Balogh, S. J. Bame, G. Erdos, R. J. Forsyth, B. E. Goldstein, J. L. Philips, and B. Tsurutani, Geophys. Res. Lett. **20**, 2327 (1993).
[40]E. J. Smith, R. G. Marsden, and D. E. Page, Science **268**, 1005 (1995).
[41]A. Balogh, E. J. Smith, B. T. Tsurutani, D. J. Southwood, R. J. Forsyth, and T. S. Horbury, Science **268**, 1007 (1995).
[42]M. Neugebauer, R. J. Forsyth, A. B. Galvin, K. L. Harvey, J. T. Hoeksema, A. J. Lazarus, R. P. Lepping, J. A. Linker, Z. Mikić, J. T. Steinberg, R. von Steiger, Y.-M. Wang, and R. Wimmer-Schweingruber, J. Geophys. Res. **103**, 14587 (1998).
[43]S. E. Gibson, D. A. Biesecker, M. Guhathakurta, J. T. Hoeksema, A. J. Lazarus, J. A. Linker, Z. Mikić, Y. Pisanko, J. T. Steinberg, B. J. Thompson, and X. P. Zhao, ''The three-dimensional coronal magnetic field during Whole Sun Month,'' to appear in Astophys. J.
[44]A. R. Breen, Z. Mikić, J. A. Linker, A. J. Lazarus, B. J. Thompson, P. J. Moran, C. A. Varley, P. J. S. Williams, D. A. Biesecker, and A. Lecinski, ''Interplanetary scintillation measurements of the solar wind during Whole Sun Month: Linking coronal and *in situ* observations,'' J. Geophys. Res. (in press).
[45]A. Posner, V. Bothmer, B. J. Thompson, H. Kunow, B. Heber, R. Muller-Mellin, A. J. Lazarus, A. Szabo, Z. Mikić, and J. A. Linker, ''In-ecliptic CIR-associated energetic particle events and polar coronal hole structures: SOHO/COSTEP observations for the Whole Sun Month campaign,'' J. Geophys. Res. (in press).
[46]M. H. Acuna, K. W. Ogilvie, D. N. Baker, S. A. Curtis, D. H. Fairfield, and W. H. Mish, Space Sci. Rev. **71**, 5 (1995).
[47]Z. Mikić and A. N. McClymont, *Solar Active Region Evolution: Comparing Models with Observations*, edited by K. S. Balasubramaniam and G. W. Simon (Astronomical Society of the Pacific, 1994), Conf. Ser. Vol. 68, p. 225.
[48]This simulation took 65 h of CPU time on a single processor of the Cray-T90 supercomputer. A real-time solution would take about 10 times longer. It may be possible to perform a real-time simulation once our code is ported to a massively parallel computer.
[49]G. L. Withbroe, Astrophys. J. **325**, 442 (1988).
[50]S. R. Habbal, R. Esser, M. Guhathakurta, and R. R. Fisher, Geophys. Res. Lett. **22**, 1465 (1995).
[51]R. Rosner, W. H. Tucker, and G. S. Vaiana, Astrophys. J. **220**, 643 (1978).
[52]J. V. Hollweg, Rev. Geophys. Space Phys. **16**, 689 (1978).
[53]S. A. Jacques, Astrophys. J. **215**, 942 (1977).